Use of Rotating Magnetic Field for Selenium Impurity Transport in Zone Refining of Tellurium and Cadmium

J. Roszmann[1], Y.C. Liu[1], S. Dost[1,2], B. Lent[1], S. Grenier[3] and N. Audet[3]

Abstract: The article presents the results of a combined numerical and experimental study of the effect of rotating magnetic field on impurity transport in a zone refining system. An impurity (selenium) with a segregation coefficient close to unity was targeted. The three-zone system previously developed was used for experiments and numerical simulations. The numerical simulations were performed for tellurium (Te) and cadmium (Cd) molten zones, but the experiments could only be carried out for the Te-system.

Keywords: Zone refining, Impurity transport, Magnetic field, Tellurium, Cadmium.

Nomenclature

B	applied rotating magnetic field intensity
ω_B	applied rotating magnetic field frequency
h and h_r	convective and radiative heat transfer coefficients
u, v, w	flow velocity components in the x-, y, z-directions
v_r, v_φ, v_z	flow velocity components in the r-, φ, z-directions
ρ	fluid density
k_L	fluid thermal conductivity
c_p	fluid specific heat
g	gravitational constant
ν	kinematic viscosity
T_{mp}	melting point
p	pressure
T and T_o	temperature and reference temperature

[1] Crystal Growth Laboratory, University of Victoria, Victoria, BC, Canada V8W 3P6
[2] Corresponding author. Tel: +1-250-721 8898; Fax: +1-250-721 6294. E-mail: sdost@me.uvic.ca
(S. Dost)
[3] 5N Plus Inc, Rue Garand, Saint-Laurent, QC, Canada H4R 2B4

β_t	thermal expansion coefficient
V_n	translation rate of the molten zone
C	selenium impurity mass concentration
C_s	selenium solid concentration
k_{se}	selenium segregation coefficient
T_f	surrounding temperature obtained from the global thermal analysis

1 Introduction

In a zone refining process, a molten zone is passed through a solid ingot. Solutes rejected by the freezing solid accumulate in the molten zone and are carried to the tail of the ingot, while solutes preferentially absorbed by the solid are transported to the leading tip of the ingot. The direction and rate of solute transport within a specific material is determined by its segregation coefficient, k_{se}. For solutes with k_{se} close to unity, such as selenium in a tellurium ingot, many zone passes are required to achieve significant mass transport.

The goal of a zone refining process is to maximize the yield and purity of product material and minimize cost. Extensive theoretical, numerical, and experimental efforts have been made to achieve this goal. (see for instance King and Brown (1992); Pfann (1966); Rodway and Hunt (1989); Wang and Kim (1977); Ho et al (1999); Spim et al (2000); Prasad et al (2002); Munirathnam et al (2005); Liu et al (2006); Zajour et al (2006); Prasad et al (2006); Haas et al (2007); Dost et al (2007); Liu et al (2008), specific contributions of these studies were discussed in detail in Liu et al (2006)). These efforts have focused mainly on enhancing the transport of impurities in the vicinity of the solidification interface and on increasing the travel rate of the molten zone. The enhancement of mass transport has been achieved by optimizing the molten zone length and shape of the molten zone. The higher travel rate has been realized by achieving higher temperature gradients in the vicinity of the solidification interface Epstein et al (1957).

A critical limiting factor that restricts the effectiveness of a zone pass is the solutal boundary layer close to the solidification interface. Convective mixing maintains a nearly uniform solute concentration throughout the liquid zone, but at the interface itself diffusion dominates solute transport, and a local peak in concentration can counteract the effect of segregation. Improved solute transport within this boundary layer would improve the effectiveness of each zone pass and significantly reduce the process cost. Recent experimental efforts to improve solute transport in tellurium using an applied electric current were unsuccessful due to the low conductivity of both liquid and solid tellurium Dost et al (2007). At the very high electric current densities required for electromigration of impurities, heat generation in the ingot

prevented suitable zones from forming.

As mentioned earlier, in order to purify impurities with a segregation coefficient close to unity, such as selenium, the passage of molten zones is not so efficient; a large number of passes are required. In the present work, the application of an applied rotating magnetic field was considered to see whether the efficiency of the zone purification process can be improved for the selenium transport by obtaining a better mixing in the molten zones.

Since the impurity removal cannot be numerically simulated over the entire zone refining process (over many passes), the removal of selenium from both tellurium and cadmium in this work was modelled numerically for only a single molten zone. In the model we selected the selenium segregation coefficient deliberately as 0.8. Although this may be slightly higher than the values suggested in phase diagrams and also calculated values from our experiments, we aimed at this selection because it is smaller than unity but large enough to allow mass transport in the molten zone to see the effectiveness of the applied magnetic fields.

The objective of the experimental part was to determine the effectiveness of an applied rotating magnetic field on overall impurity transport. Experiments were conducted for the entire zone refining process (after three passes) of tellurium. Results show little effect of magnetic field in this system. Although the numerical modelling suggested a greater effect might be observed in cadmium, the present zone refiner system used for the experimental study was not capable of producing reliably stable molten zones in cadmium due to its larger thermal conductivity (see Liu et al (2006) for thermal characteristics of a cadmium system). The presence of the magnetic field generator around the molten zone made impossible to provide the required cooling (heat shield) normally used in the cadmium zone refining system to have stable zones (to keep the zones separate). There is not a sufficient room between the molten zone and the field generator as seen in Figure 1. This requires the design of a new zone refining set up with a proper field generator which is presently beyond our means.

2   The numerical simulation model

A single molten zone was considered for numerical simulation mainly because in experiments one zone at a time was translated under an applied magnetic field, and it may also not feasible (possible) to simulate numerically the entire process of several passes.

A schematic view of the entire system and also the model domain (molten zone) along with the coordinate system used are given in Figure 2. The molten zone (liquid phase) is assumed to be an incompressible, viscous Newtonian fluid with a
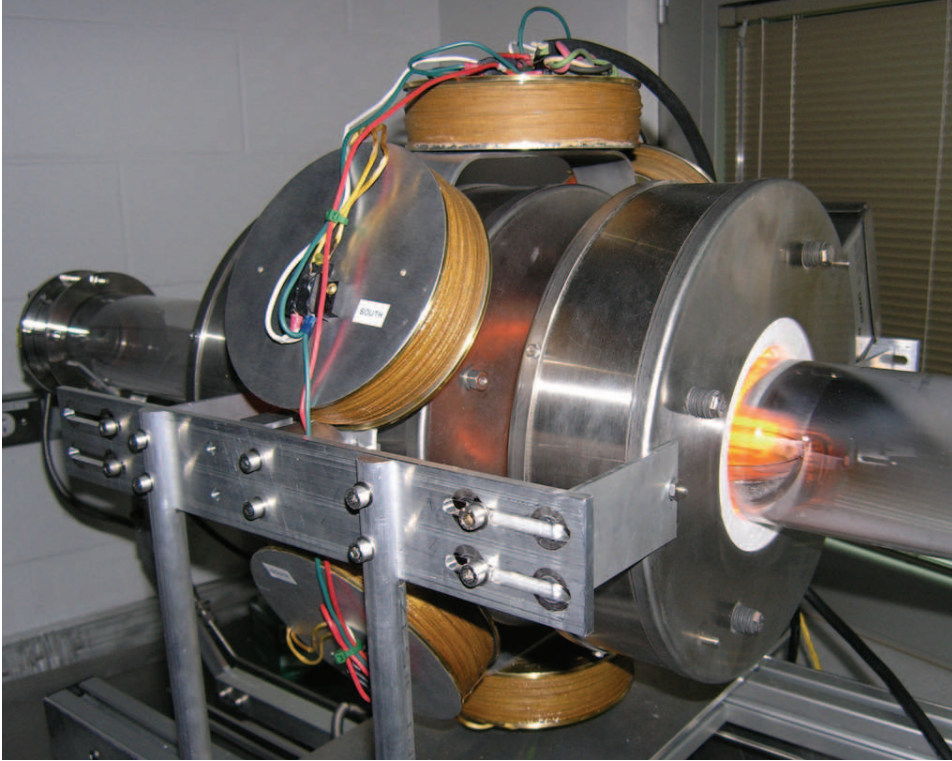
Figure 1: CGL Zone refiner fitted with rotating magnetic field coils.

low concentration of a selected selenium impurity.

2.1   Field Equations

The governing equations of the liquid phase are the continuity, momentum, energy, and mass transport equations, given respectively by

Continuity

$$\frac{\partial u}{\partial x} + \frac{\partial v}{\partial y} + \frac{\partial w}{\partial z} = 0 \tag{1}$$

Momentum

$$\frac{\partial u}{\partial t} + u\frac{\partial u}{\partial x} + v\frac{\partial u}{\partial y} + w\frac{\partial u}{\partial z} = \nu\left(\frac{\partial^2 u}{\partial x^2} + \frac{\partial^2 u}{\partial y^2} + \frac{\partial^2 u}{\partial z^2}\right) - \frac{1}{\rho_L}\frac{\partial p}{\partial x} + \frac{F_x^M}{\rho_L} \tag{2}$$
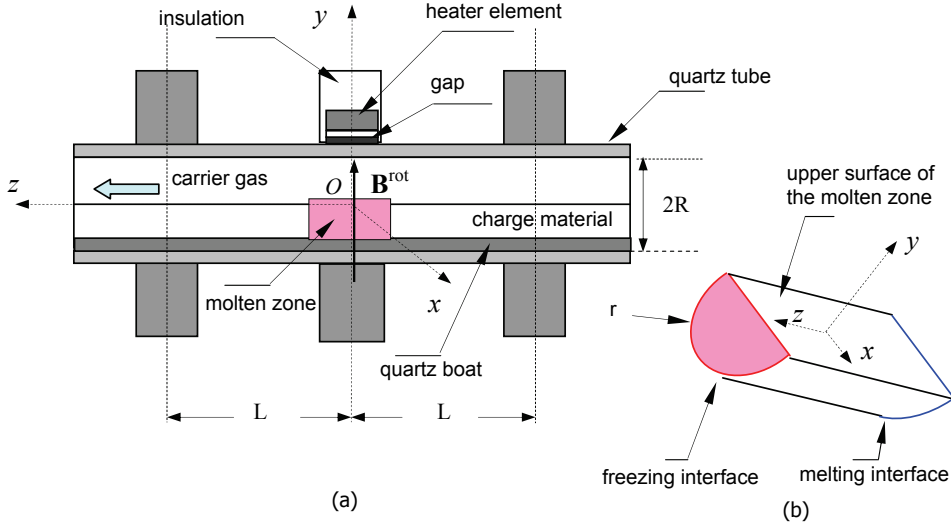
Figure 2: Schematic view of the three-zone refining system (a), and the modelled single molten zone with the coordinate system used (b). In the figure R = 90mm, r = 70mm, L = 140mm.

$$\frac{\partial v}{\partial t} + u\frac{\partial v}{\partial x} + v\frac{\partial v}{\partial y} + w\frac{\partial v}{\partial z}$$

$$= \nu\left(\frac{\partial^2 v}{\partial x^2} + \frac{\partial^2 v}{\partial y^2} + \frac{\partial^2 v}{\partial z^2}\right) - \frac{1}{\rho_L}\frac{\partial p}{\partial y} - g\beta_t\left(T - T_0\right) + \frac{F_y^M}{\rho_L} \quad (3)$$

$$\frac{\partial w}{\partial t} + u\frac{\partial w}{\partial x} + v\frac{\partial w}{\partial y} + w\frac{\partial w}{\partial z} = \nu\left(\frac{\partial^2 w}{\partial x^2} + \frac{\partial^2 w}{\partial y^2} + \frac{\partial^2 w}{\partial z^2}\right) - \frac{1}{\rho_L}\frac{\partial p}{\partial z} + \frac{F_z^M}{\rho_L} \quad (4)$$

Energy

$$\frac{\partial T}{\partial t} + u\frac{\partial T}{\partial x} + v\frac{\partial T}{\partial y} + w\frac{\partial T}{\partial z} = \frac{k_L}{\rho_L\, c_p}\left(\frac{\partial^2 T}{\partial x^2} + \frac{\partial^2 T}{\partial y^2} + \frac{\partial^2 T}{\partial z^2}\right) \quad (5)$$

Mass transport for solute

$$\frac{\partial C}{\partial t} + u\frac{\partial C}{\partial x} + v\frac{\partial C}{\partial y} + w\frac{\partial C}{\partial z} = D_L\left(\frac{\partial^2 C}{\partial x^2} + \frac{\partial^2 C}{\partial y^2} + \frac{\partial^2 C}{\partial z^2}\right) \quad (6)$$

Detailed derivations of the rotating magnetic body force components in the above equations can be found in Yildiz and Dost (2007). In the absence of the contribution

of the induced electric field, these magnetic force components (time-averaged) are given in cylindrical coordinates by

$$F_r^M = -\frac{B^2 \sigma_E}{2} v_r,$$
$$F_\varphi^M = \frac{1}{2} \sigma_E B^2 (\omega_B r - v_\varphi),$$
$$F_z^M = -\sigma_E B^2 v_z \tag{7}$$

The needed Cartesian components, i.e. F_x^M, F_y^M, and F_z^M in Eqs.(2)-(4) are numerically computed from the above components.

2.2 *Boundary and interface conditions*

The following boundary and interface conditions are used in the model.

At the melting interface:

We assume no-slip boundary conditions for the flow field, the interface temperature at the melting point, and an equilibrium impurity concentration, i.e.,

$$u = 0, \quad v = 0, \quad w = 0, \text{ and } T = T_{mp} \tag{8}$$

At the solidification interface:

Similarly, for the flow field and temperature we use

$$u = 0, \quad v = 0, \quad w = 0, \quad T = T_{mp} \tag{9}$$

and the mass balance for the selenium impurity concentration is

$$\frac{\rho}{\rho_s} D \frac{\partial C}{\partial z} = C(k_{se} - 1) V_n \text{ with } k_{se} = C_s / C \tag{10}$$

At the liquid/gas interface:

The flow field includes the contribution of surface tension as

$$\frac{\partial u}{\partial y} = \frac{\frac{d\gamma}{dT}}{\mu} \frac{\partial T}{\partial x}, \quad v = 0, \quad \frac{\partial w}{\partial y} = \frac{\frac{d\gamma}{dT}}{\mu} \frac{\partial T}{\partial z} \tag{11}$$

and energy balance and concentration conditions are written respectively as

$$q = h(T - T_f) + h_r(T^4 - T_f^4), \quad \frac{\partial C}{\partial y} = 0 \tag{12}$$

At the solid ingot surface:

$$u = 0, \quad v = 0, \quad w = 0,$$

$$q = h(T - T_f) + h_r(T^4 - T_f^4), \quad \frac{\partial C}{\partial y} = 0 \tag{13}$$

The heat transfer coefficients at the exterior surfaces of the zone were chosen to closely fit the temperature profile obtained for the ingot from the global thermal analysis Liu et al (2006, 2008). In the computations we used the values of T_f = 20C = 293K, h = 100W/(m^2 K), $h_r = 3.2 \times 10^{-8} W/(m^2 K^4)$, $d\gamma/dT = 6.0 \times 10^{-5} N/(mK)$, and V_n = translating rate = 2 cm/hr. The remaining physical parameters related to mass and momentum transfer of *Cd* and *Te* systems are presented in Table 1. All other physical properties related to *Te*, *Cd*, quartz, heaters, and insulator, and the geometrical and operating parameters can be found in Tables 1-2 of Ref. Liu et al (2006).

Table 1: Physical parameters

Parameter (symbol)	Value	Unit	Citation
Impurity diffusion coefficient in *Cd* and *Te* melts (*D*)	5.0×10^{-9}	m^2/s	estimated
Impurity segregation coefficient (*k_{se}*)	0.8		selected
Electrical conductivity (σ_E) of *Cd*	3.7×10^7	$(\Omega m)^{-1}$	Budgen (1924)
Electrical conductivity (σ_E) of *Te*	3.3×10^5	$(\Omega m)^{-1}$	estimated
Applied rotating magnetic field intensity (*B*)	50	Gauss	
Rotating magnetic field frequency used in the model (ω_B)	0, 30, 90, 270	Hz	
Initial impurity concentration selected in the model (C_0)	0.001		

3 Numerical solution

The governing equations of the model are solved numerically by the commercial CFX software package of AEA technology. Several user-defined Fortran subroutines were developed to deal with the complex temperature boundary conditions and the contribution of the applied magnetic field. Time derivatives were calculated by the backward finite difference algorithm. The hybrid-differencing scheme, a variation of the upwind differencing method, is the default setting in CFX and

Table 2: ICP analysis for the selenium impurity

Test #	Ingot mass (kg)	Selenium impurity content (PPM,m)				Calculated k_{eff}
		Sample 1	Sample 2	Sample 3	Sample 4	
29	2.5	22	13.7	9.7	0	-
30	2.469	71.7	34.7	14.9	7.2	0.494
31	2.468	66.5	36.3	14.9	7.2	0.494
32	2.476	71.6	35.0	15.2	7.6	0.505
33	2.467	61.5	36.8	15.5	6.5	0.474

was used for the discretization of the convective terms. Higher-order differencing schemes are found to be less robust for the present model. The mesh size $80 \times 80 \times 80$ (in the *x*-, *y*-, and *z*-directions, respectively) is demonstrated to be sufficient for an accurate and stable solution.

4   Numerical simulation results

The computations were carried out for the first cycle of the *Cd* and *Te* systems. Studying one cycle is considered sufficient to determine the contribution of an applied rotating magnetic field. The contribution of induced electric field is neglected in the model. For the selenium impurity, we set the initial liquid concentration value at 0.001. In order to determine the sensitivity of computations, we varied this value from 0.0001 to 0.01. Results showed that the computational procedure is not sensitive to the variation of the initial concentration value, and 0.001 was a reasonable choice.

Details of the thermal analysis of the entire system and also that of molten zones can be found in refs Liu et al (2006) and Liu et al (2008). For the sake of completeness, we only present here the associated dimensionless numbers: Ra = 1.5×10^6, Ma = 4.4×10^4, Pr = 0.015, Sc = 296.

Due to the low electric conductivity of the Te-system and perhaps also strong convection in the Te-molten zone (see Liu et al (2008) for flow patterns), the simulation results showed no notable difference in the thermal, flow velocity and concentration fields compared with those in the absence of an applied rotating magnetic field. Therefore, the computed flow velocity and concentration fields in the molten zone are presented only for the *Cd* system, with and without the application of a rotating magnetic field (Figure 3).

The computed flow velocity field (left column) and the concentration field (right column) in the vertical plane (passing through the $z-$axis) at *t* = 300 s are shown in Figure 3a in the absence of an applied rotating magnetic field, in Figure 3b for an

(a) $B = 0$

(b) $B = 50$ G and $\omega_B = 30$ Hz
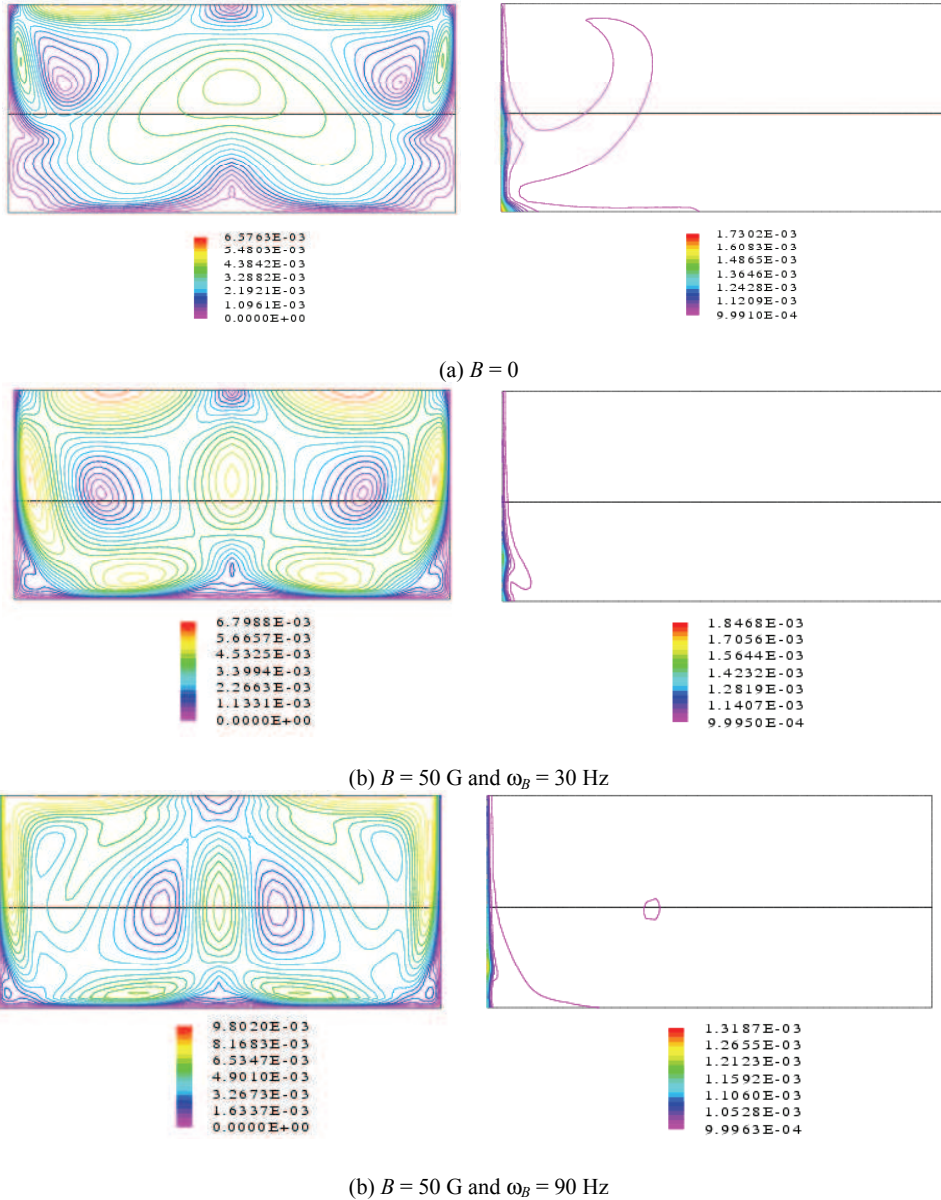

(b) $B = 50$ G and $\omega_B = 90$ Hz

Figure 3: Computed flow velocity (left column) and impurity concentration (right column) fields (in Cd) in the vertical axial plane along the centre of the liquid zone at $t = 300$ s: (a) at $B = 0$ (no magnetic field), (b) $B = 50$ G and $\omega_B = 30$ Hz, and (c) $B = 50$ G and $\omega_B = 90$ Hz.
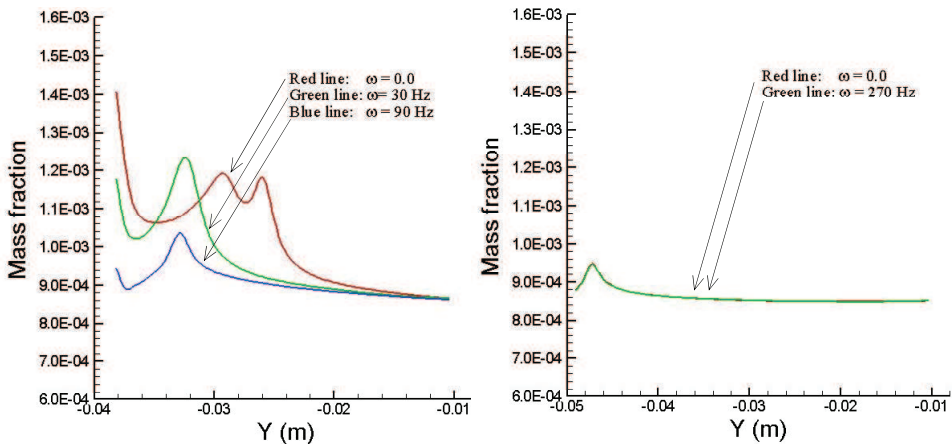
Figure 4: Solid concentration distribution along the vertical (y-) direction at the middle of the solidification interface for the *Cd* system (left) under three different RMF frequencies, and for the *Te*-system (on right) for a very high frequency of 270 Hz.

applied rotating magnetic field intensity $B = 50$ G and frequency $\omega_B = 30$ Hz, and in Figure 3c for $B = 50$ G and $\omega_B = 90$ Hz. In the figures, the left vertical boundary is the freezing interface and the right is the melting interface. The comparison of Figures 3a,b shows that the applied rotating magnetic field (at $B = 50$ G and $\omega_B = 30$ Hz) alters the flow field, giving rise to enhanced mixing in the bottom half of the molten zone and in the regions near the melting and solidifying interfaces. The flow field near the free surface seems unaffected due to the strong Marangoni convection in this region. The impurity concentration distribution is also affected leading to a more uniform distribution as seen on the right column.

At the higher frequency level ($\omega_B = 90$ Hz) the change in the flow velocity field is more prominent including the region near the free surface (Figure 3c). However, the concentration is less uniform compared with that at $\omega_B = 30$ Hz, implying that the frequency level about 30 to 40 Hz is sufficient.

In order to have a more quantitative visualization for the impurity concentration distribution, the computed solid impurity mass fraction along the vertical axis at the middle of the solidifying interface is presented in Figure 4a for three frequencies: $\omega_B = 0$, 30, 90 Hz for Cd and for $\omega_B = 270$ Hz for Te. As seen, the application of a rotating magnetic field alters the impurity concentration distribution in the Cd-system. As mentioned earlier, however, the effect of magnetic field is not significant in the Te-system as seen in Figure 4b, which is qualitatively supported by

experiments as discussed in the next section. Figure 4 shows the results of numerical simulations carried out to examine the effect of applied magnetic field on the impurity distribution in a molten zone of the system. This was the objective. This prediction cannot be determined by characterizing the processed samples.

5 Experimental results

A series of experiments was carried out using the University of Victoria's CGL zone refiner (Haas et al (2007)). As mentioned earlier, the selenium impurity was targeted because its segregation coefficient in *Te* is close to unity, and thus it is difficult to remove such an impurity using the standard zone refining technique. The objective of the experimental work was to determine the effect of a rotating magnetic field on selenium segregation in *Te* using a production scale system, i.e., after several passes of zones (Figure 1). In the experiments three passes were considered sufficient for the objective of this work.

A single experiment was conducted under a rotating magnetic field using tellurium from 5N Plus lot# Te-HPO-60923. The distribution of selenium in the resulting ingot suggested a surprisingly strong improvement when compared to the results of the electromigration experiments which used the same feed material and were published in Dost et al (2007), so four more experiments were conducted using tellurium doped with 35 ppm selenium. The feed material was provided in two 5 kg bags by 5N Plus and was not mixed prior to the experiments. Two experiments were conducted with no applied magnetic field, and then two more were carried out under a 0.6 mT field rotating at 100 Hz. In all experiments, one zone was passed three times through the entire ingot at 20 mm/hr. The CGL zone refiner has three heaters. Rotating magnetic field coils were mounted only on the middle heater, and this heater was used to produce the molten zone with the two outside heaters set below the melting point. The magnetic field ran continually throughout the melt, solidification and zone passing phases of each experiment, and hydrogen at atmospheric pressure flowed above the ingot at 200 mL/min.

The selenium distributions in the five ingots are tabulated in Table 2 and plotted in Figure 5.

Figure 5 shows the impurity distribution after three passes of zones, at the end of the process, by characterizing the processed ingot by taking samples of slices at specific location. The impurity level is determined by analyzing these sliced samples (average value). It is clear that mass transport did purify the tip of the ingot in all cases; however, the four experiments conducted with identical feed material showed no observable effect due to the applied rotating magnetic field

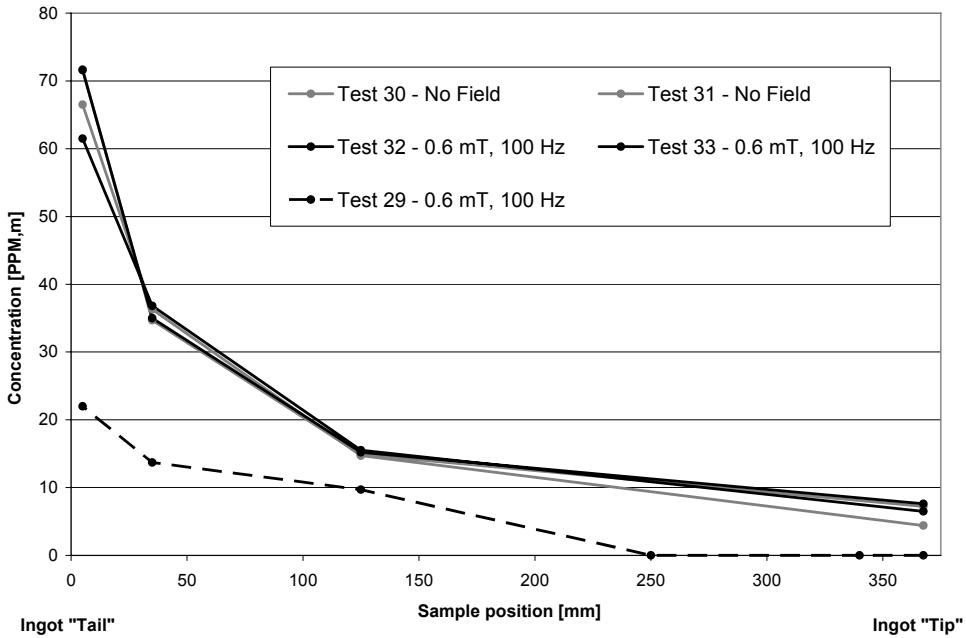The effective segregation coefficient(s) k_{eff} can be calculated using the well-known

Figure 5: ICP analysis for the selenium impurity distribution. Note from Table 2 that the results of tests 30 and 32 are almost identical, thus they appear as a single plot in the figure.

Pfann Pfann (1966) equation:

$$\frac{C_n(a)}{C_o} = 1 - (1-k)e^{-ka}\left[n - \sum_{s=1}^{n-1}(n-s)\,k^{s-1}e^{-sk}\right.$$
$$\left.\frac{(s+a)^{s-2}}{s!}\left[a\,(s-1) + (1-ka)\,(s+1)\right]\right] \quad (14)$$

which gives the concentration as a function of distance a (in zone lengths) along the ingot after n passes. We used this equation to solve for k_{eff}, and the calculated values are presented in Table 2 in the last column.

As can be noted, these values are smaller (around 0.5) than the selected value of 0.8 in the model. However, there are a couple of very important issues that should be noted. First, this function is only valid in the region (0 < x < L-n*l). That is, only up to *n* zone lengths from the end of the ingot since the equation does not include the effect of impurities piling up against the end of the ingot. Because we tested mostly the dirty end of the ingot, all of our data comes from this forbidden region

except for those measurements taken at the very tip of the ingot. To calculate k_{eff} by this way, one can therefore rely on only one concentration measurement per experiment.

Furthermore, more importantly these calculated values include the removed *Se* by evaporation under the effect of a carrier gas (Figure 2). Because we are comparing a single concentration measurement to the original selenium concentration, one cannot compensate for the evaporation of selenium during the experiment.

6   Conclusion

The results of a combined numerical and experimental study examining the effect of an applied rotating magnetic field on impurity transport in a zone refining system show that under the experimental and modelling conditions considered, the flow velocity field intensity in the *Cd*-molten zone becomes higher at higher magnetic field frequency levels, and enhances mixing in the melt. While the concentration field at the top of the molten zone appears unaffected due to the strong contribution of Marangoni convection, the applied rotating magnetic field gives rise to stronger flow velocity intensity at the bottom of the molten zone leading to enhanced impurity transport. The effect of an applied magnetic field in the *Te*-system seems not significant due to low conductivity of tellurium and strong convection in the *Te*-molten zone.

The experimental results support the numerical conclusion that magnetic fields have little effect in the tellurium system. Beyond this, no direct comparison can be made because the numerical analysis performed cannot predict a final impurity distribution or segregation coefficient, and the experimental study cannot not test for velocity or concentration fields in the liquid molten zone. Because of this, a direct comparison is not possible, only the end results. The qualitative conclusion that RMF does not help tellurium zone refining, which is supported by both modeling and experimental studies.

References

Budgen, N.F. (1924): *Cadmium: Its Metallurgy, Properties and Uses*, C. Griffin & company, limited.

Dost, S.; Liu, Y.C.; Haas, J.; Roszmann, J.; Grenier, S.; Audet, N. (2007): *J. Crystal Growth*, 307, 211.

Epstein, A.S.; Fritzsche, H.; Lark-Horovitz (1957): *Physical Review*, 107(2), 412.

Haas, J.; Dost, S.; Liu, Y.C. (2007): *Scientia Iranica*, 14(5), 474.

Ho, C.D.; Yeh, H.M.; Yeh, T.L. (1999): *Separation and Purification Technology*, 15, 69.

King, C.A.; Brown, S.V. (1992): *Rev. Sci. Instrum.*, 63, 3187.

Liu, Y.C.; Moss, R.; Dost, S. (2006): *J. Crystal Growth*, 293, 146.

Liu, Y.C.; Dost, S.; Audet, N.; Grenier, S.; Haas, J. (2008): *Int. J. Materials and Products Technology*, 32(1), 1.

Munirathnam, N.R.; Prasad, D.S.; Rao, J.V.; Prakash, T.L. (2005): *Bull. Mater. Sci.*, 28, 209.

Pfann, W.G. (1966): *Zone Melting*, New York: John Wiley.

Prasad, D.S.; Sudheer, C.; Munirathnam, N.R.; Prakash, T.L. (2002): *Bull. Mater. Sci.*, 25, 545.

Prasad, D.S.; Munirathnam, N.R.; Rao, J.V.; Prakash, T.L. (2006): *Materials Letter*, 60, 1875.

Rodway, G.H.; Hunt, J.D. (1989): *J. Crystal Growth*, 97, 680.

Spim, J.A.J.; Bernadou, M.J.; Garcia, A. (2000): *J. Alloys Compounds*, 298, 299.

Wang, J.H.; Kim, D.H. (1977): *J. Crystal Growth*, 173, 201.

Yildiz, E.; Dost, S. (2007): *J. Crystal Growth*, 303(1), 279.

Zajour, A.; Zahraman, K.; Roumie, M.; Charara, J.; Fawaz, A.; Lmai, F.; Hage-Ali, M. (2006): Purification of Tellurium to Nearly 7N Purity, *Material Science and Engineering B: Solid-state Materials for Advanced Technology*, 131, 54.